International Journal of Mass Spectrometry 459 (2021) 116468

Contents lists available at ScienceDirect

International Journal of Mass Spectrometry

journal homepage: www.elsevier.com/locate/ijms

Chemical dynamics simulations of collision induced dissociation of deprotonated glycolaldehyde

Anchal Gahlaut, Manikandan Paranjothy*

Department of Chemistry, Indian Institute of Technology Jodhpur, Jodhpur, 342037, Rajasthan, India

ARTICLE INFO

Article history:
Received 11 September 2020
Received in revised form
28 October 2020
Accepted 29 October 2020
Available online 7 November 2020

Keywords:
Direct dynamics
Glycolaldehyde anion
Formose reaction
Density functional theory
Collision induced dissociation

ABSTRACT

First step of formose or Butlerov reaction involves C—C bond formation between two formaldehyde molecules resulting in glycolaldehyde. This reaction happens under basic conditions in solution. A tandem mass spectrometry investigation of dissociation of deprotonated glycolaldehyde in the gas phase, to study the formose reaction in a retro-synthetic point of view, has been reported. In the present work, we have carried out electronic structure theory calculations and quasi-classical direct chemical dynamics simulations to model the gas phase dissociation of the conjugate base of glycolaldehyde. The dynamics simulations were performed *on-the-fly* using the hybrid density functional B3LYP theory with the 6-31+G* basis set under collision induced dissociation (CID) conditions. Trajectories were launched with two different deprotonated forms of glycolaldehyde for a range of collision energies mimicking experiments. Reverse formose reaction was observed primarily from the slightly higher energy isomer via a non-statistical pathway. Intramolecular hydrogen transfer was ubiquitous in the trajectories. Simulation results were compared with experiments and detailed atomic level dissociation mechanisms are presented.

1. Introduction

In the formose or Butlerov reaction, formaldehyde oligomerizes to form carbohydrates and this reaction is considered to be the source of prebiotic sugar formation on early Earth [1]. The first step of this reaction involves the formation of glycolaldehyde from two formaldehyde molecules.

$$2HCHO \rightarrow CH_2OHCHO \quad (1)$$

In solution, this reaction has been proposed to occur between a deprotonated formaldehyde (HCO^- anion formed under basic conditions) and a neutral formaldehyde molecule [2]. Studies have shown that the proposed mechanism was not entirely correct and further experimental and computational investigations of the formose reaction have been reported [3—9].

Glycolaldehyde (GA) is the simplest possible sugar which is also known as diose. GA has been detected in the atmosphere as a product of photochemical oxidation of volatile organic molecules such as ethene and isoprene [10—12] in addition to direct emission from biomass burning [13,14]. Decay of GA in the troposphere occurs mainly via OH radical reaction and photochemical decomposition. Photolysis reaction of GA has been investigated in solution [15] and in the gas phase [16,17]. Porterfield et al. [18], have studied the pyrolysis of GA and products such as H, CO, HCHO, CH_2CO, etc. were identified using photoionization mass spectrometry. More than two hundred organic molecules have been detected in the interstellar medium and GA is the only sugar among them [19—23]. GA combines with propenal resulting in ribose, a central component of RNA, and hence GA is considered to be a precursor of RNA [24]. Even though GA has been detected in space, no well established mechanism for the gas phase formation of GA is available in the literature. For instance, formation of protonated GA from association reaction between formaldehyde and protonated formaldehyde in the interstellar medium was considered [7] but later this reaction was shown to be inefficient [8,9]. Electronic structure theory studies have shown that metal ion catalyzed and hydrogen bond mediated dimerization of formaldehyde to form glycolaldehyde are nearly barrier-less processes [25].

Relevant to the formose reaction, gas phase fragmentation of deprotonated GA, $C_2H_3O_2^-$ was investigated by Uggerud and coworkers [26]. From a retro-synthetic point of view, dissociation of

* Corresponding author.
E-mail address: pmanikandan@iitj.ac.in (M. Paranjothy).

https://doi.org/10.1016/j.ijms.2020.116468
1387-3806/

the conjugate base of GA forming HCO^- + HCHO products was investigated using tandem mass spectrometry under collision induced dissociation (CID) conditions [27]. Experiments were carried out for a range of collision energies (0.2–20 eV) and the HCO^- + HCHO products were not identified as primary decomposition products of deprotonated GA. Signal at m/z = 31, corresponding to the reaction $C_2H_3O_2^- \rightarrow CO + CH_3O^-$, was the dominant peak in the mass spectrum. Other than this work, there are no studies in the literature reporting the fragmentation chemistry of the deprotonated GA. In the present work, we have investigated the dissociation chemistry of deprotonated GA using detailed electronic structure theory calculations and classical direct chemical dynamics simulations [28,29] to model the collision induced dissociation experiments by Uggerud and co-workers [26]. The simulations were performed by *on-the-fly* integration of classical trajectories using potentials and gradients computed from density functional theory. The trajectory initial conditions were selected to mimic single collision conditions in the gas phase. A variety of decomposition products including HCO^- + HCHO were identified. Simulation results were compared with previously reported CID experiments and detailed atomic level dissociation mechanisms are presented. The article is organized as follows. Computational Methodology is presented in the next Section followed by a detailed Results and Discussion. The article is summarized in the last Section. Supporting Information containing optimized coordinates of stationary points, reaction schemes, etc. is provided.

2. Computational methods

Electronic structure calculations and the direct classical trajectory integrations were performed using the density functional B3LYP method utilizing the 6-31+G* basis set. This level of theory was selected because of the accuracy [26] and the limited computational costs associated with the method. A comparison of stationary point energies computed using B3LYP/6-31+G* method and higher level methods is presented in the Supporting Information. Deprotonation of GA (CH_2OHCHO) can occur at three positions viz., carbonyl carbon (CH_2OHC^-O, 1X), the second carbon atom ($^-CHOHCHO$, 1C), and the hydroxyl group (CH_2OCHO^-, 1O). Geometries of these species were optimized using the B3LYP/6-31+G* method and the results are shown in Fig. 1. 1C is the lowest energy isomer (0.0 kcal/mol) followed by 1O (4.0 kcal/mol) and 1X (21.6 kcal/mol). Potential energy profiles of possible dissociation pathways (based on previous work [26]) of deprotonated GA were characterized using B3LYP/6-31+G* method. All the stationary points were geometry optimized and normal mode frequency calculations were performed to differentiate an equilibrium point from a transition state. Intrinsic reaction coordinate (IRC) calculations were performed to ascertain whether a given transition state connects correct product(s) with the reactant. The results are summarized in Fig. 2 wherein the given energies (in kcal/mol) are relative to 1C without zero point energy corrections. Optimized geometries of various stationary points on the dissociation energy profile of deprotonated GA are provided in the Supporting Information. Quantum chemistry calculations reported in the present work were performed using the electronic structure theory package NWChem [30].

Collision induced dissociation experiments of deprotonated GA were modeled using Born-Oppenheimer direct chemical dynamics simulations [28,29] to establish atomic level reaction mechanisms. Classical trajectories were initiated from 1C and 1O isomers and they were excited by collision with an Ar atom. Vibrational and rotational energies of the reactant species were selected from 300 and 75 K Boltzmann distributions, respectively, using standard algorithms [27,31]. An initial separation of 10.0 Å was kept between the reactant molecule and the Ar atom and the collision occurred with an impact parameter of 0.0 Å. Reactant molecule was rotated randomly in each trajectory allowing for collisions at different sites of the molecule. Relative translational energy E_{rel} between the center-of-mass of the reactant molecule and the colliding Ar atom was fixed at four different values viz., 2, 5, 9, and 13 eV. These E_{rel} values were selected based on experiments [26]. Trajectories were integrated till 3 ps or until reaction products were separated by a distance of 12.0 Å using a 6^{th} order Symplectic integrator [32,33] with a step-size of 0.5 fs. These simulation conditions were sufficient enough to maintain a good energy conservation in the trajectories. Total energy E_{tot}, which is the conserved energy of the whole system, in the trajectories were approximately 75, 148, 240, and 330 kcal/mol at E_{rel} = 2, 5, 9, and 13 eV, respectively, for the selected initial conditions. At each E_{rel}, 100 trajectories were generated which amounts to a total of 800 direct dynamics trajectories. Total energy in the trajectories was conserved within E_{tot} ± 1.0 kcal/mol. Trajectories were analyzed for establishing reaction pathways and mechanisms. The direct dynamics calculations were performed using the general chemical dynamics program VENUS [34,35] coupled [36] with NWChem. Default convergence parameters available in the NWChem program [30] were used in the dynamics simulations.

3. Results

3.1. Potential energy surface

It can be seen from Table 1 of Supporting Information that the stationary point energies on the dissociation energy profile of deprotonated GA calculated using B3LYP/6-31+G* theory are not

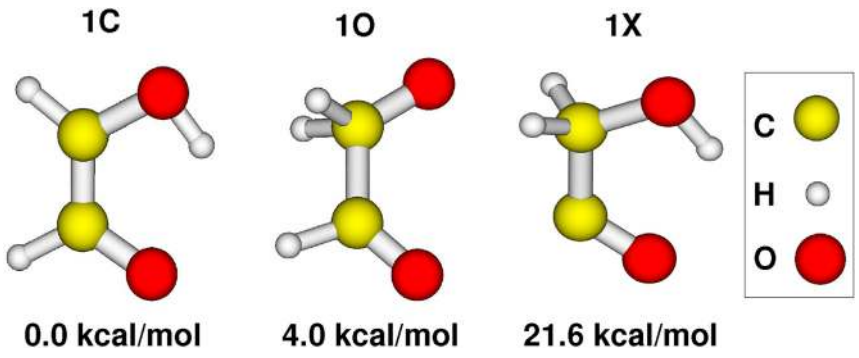

Fig. 1. Optimized geometries and relative energies of deprotonated glycolaldehyde. Energies are relative to the lowest energy 1C isomer without zero point energy corrections. Color coding used for different atoms are also shown. (For interpretation of the references to colour in this figure legend, the reader is referred to the Web version of this article.)

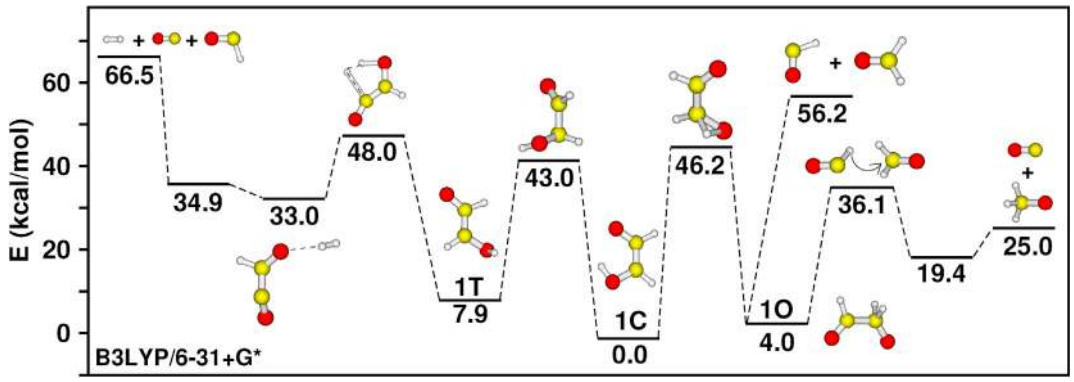

Fig. 2. Potential energy profiles of dissociation of deprotonated GA computed using B3LYP/6-31+G* level of electronic structure theory. The given energies (in kcal/mol) are relative to that of 1C and zero point energy not corrected.

Table 1
Fractions of Trajectories Showing Various Pathways Following Collisional Activation of deprotonated GA. The Number Below a Given Fraction is the Error Bar.

		1C					1O	
Pathway	2 eV	5 eV	9 eV	13eV	2 eV	5 eV	9eV	13eV
$HCHO + HCO^-$ (m/z = 29)	0	0	1 (1.0%)	1 (1.0%)	0	53 (5.0%)	77 (4.2%)	77 (4.2%)
$HCHO + CO + H^-$ (m/z = 1)	0	0	2 (1.4%)	2 (1.4%)	0	0	10 (3.0%)	16 (3.7%)
$CO + H_2 + HCO^-$ (m/z = 29)	0	0	1 (1.0%)	3 (1.7%)	0	0	1 (1.0%)	3 (1.7%)
$H_2O + O = C = CH^-$ (m/z = 41)	0	0	15 (3.6%)	29 (4.5%)	0	0	0	0
$CH_2 = C = O + OH^-$ (m/z = 17)	0	0	12 (3.3%)	37 (4.8%)	0	0	0	1 (1.0%)
$CH_2 + CO + OH^-$ (m/z = 17)	0	0	0	3 (1.7%)	0	0	0	0
GA ↔ GA (m/z = 59) (hydride transfer)	40 (4.9%)	65 (4.8%)	37 (4.8%)	17 (3.8%)	19 (3.9%)	21 (4.1%)	5 (2.2%)	0
$2CO + H_2 + H^-$ (m/z = 1)	0	0	0	2 (1.4%)	0	0	1 (1.0%)	0
$CO + {}^-CH_2OH$ (m/z = 31)	0	0	0	3 (1.7%)	0	0	0	0
$CO + CH_3O^-$ (m/z = 31)	0	0	0	0	0	4 (2.0%)	3 (1.7%)	2 (1.4%)
$(CHO)_2 + H^-$ (m/z = 1)	0	0	2 (1.4%)	1 (1.0%)	0	0	2 (1.4%)	0
$2CHO + H^-$ (m/z = 1)	0	0	0	0	0	0	0	1 (1.0%)
no reaction	60 (4.9%)	35 (4.8%)	30 (4.6%)	2 (1.4%)	81 (3.9%)	22 (4.1%)	1 (1.0%)	0
total	100	100	100	100	100	100	100	100

much different from those computed using higher level theories. Fig. 2 shows the potential energy profile computed using B3LYP/6-31+G* theory and a brief discussion is given here. The reaction of interest (deprotonated GA → HCO^- + HCHO) occurs from the 1O isomer and a direct reaction path from the lowest energy 1C isomer does not exist. The reaction is exoergic by 56.2 kcal/mol with respect to 1C. From 1O, the reaction is barrier-less and exoergic by 52.2 kcal/mol. Intramolecular hydrogen transfer resulting in 1O from 1C has a barrier of 46.2 kcal/mol and the torsional rotation of C–C resulting in the geometrical isomer 1 T requires energy of 43.0 kcal/mol. Dissociation of 1O forming CH_3O^- + CO and dehydrogenation of 1C leading to HCO^- + CO + H_2 products are also shown in Fig. 2. Transition state for the CH_3O^- + CO product formation has an energy of 32.1 kcal/mol with respect to 1O. The HCO^- + CO + H_2 products have high energy in comparison to HCO^- + HCHO and CH_3O^- + CO products.

3.2. Direct dynamics

In the dynamics simulations, a variety of reaction products were observed and a summary is given in Table 1. Along with the trajectory fractions, the associated error bars are also provided. For both the 1C and 1O isomers, the reactivity increased with increasing collision energy. Detailed discussion of the dynamics results are given below.

3.3. Dynamics of 1C

As shown in Table 1, reactivity (defined as the dissociation or isomerization following collision with Ar atom before the trajectory stopping criterion was reached) for the 1C isomer was observed in 40, 65, 70, and 98 trajectories at E_{rel} = 2, 5, 9, and 13 eV, respectively. Primary dissociation of 1C observed in the simulations was that of C–O bond (involving O of the hydroxyl group, see Fig. 1) resulting in the products H_2O + $HCCO^-$ (m/z = 41) or OH^- (m/

z = 17) + CH_2CO. In these reactions, the C–O bond dissociation is associated with intramolecular hydrogen (hydride) transfer. These reactions have not been reported earlier. Schemes for various reactions observed in the simulations are presented in the Supporting Information. Electronic structure calculations at the B3LYP/6-31+G* level of theory were performed to characterize these reaction pathways and the results are shown in Fig. 3(a). The H_2O elimination channel is endoergic (by 19.5 kcal/mol) and the reaction pathway has a transition state with energy of 69.8 kcal/mol relative to 1C. At E_{rel} = 9 and 13 eV, 15 and 29 trajectories, respectively, showed dissociation via this pathway. The ketene channel (CH_2CO + OH^-) has a reaction energy of 40.8 kcal/mol. Attempts to find a transition state for this pathway was unsuccessful. A total of 12 (9 eV) and 40 (13 eV) trajectories followed the ketene channel. Ketene has been observed in the flash pyrolysis of glycolaldehyde molecule [18]. In a small number of trajectories (3 out of 40, 13 eV), ketene underwent subsequent dissociation resulting in CH_2 + CO. Ground state dissociation of ketene is known to be barrier-less and endoergic [37]. An important observation here is that the above mentioned two reactions occurred primarily via shattering [38] and they are known as Fast Fragmentation Events [39] (FFEs) i.e., reaction occurred upon collision or within a very short time following the collision. In a shattering mechanism, the molecule does not have enough time for the excitation energy to randomize among the modes of the molecule and this is a non-statistical reaction pathway [38]. Shattering mechanism has been identified in the collision induced dissociation of CH_3SH^+, $CH_3SCH_3^+$ and $Cr^+(CO)_6$ molecules [40–43]. For the H_2O elimination pathway, the collision directly pushes the 1C molecule into the transition state configuration. Only in a very small number of trajectories, a finite time gap was observed between collision and the reaction. Previous studies [38] have shown that the shattering fragmentations can be overestimated in simulations in comparison to non-shattering mechanisms.

In a large fraction of the trajectories, intramolecular hydrogen transfer between the two O atoms was observed. This fraction is largest in the 5 eV simulation. The barrier for this reaction is 9.6 kcal/mol and the energy profile is shown in Fig. 3(a). In some of the dissociating trajectories discussed above, intramolecular hydrogen transfer occurred prior to dissociation. Note that such trajectories are not shattering type trajectories. The primary reaction of interest (GA → HCHO + HCO^-) was observed in negligible number of trajectories in these simulations. As can be seen from Fig. 2, there is no direct reaction path from 1C to HCHO + HCO^-. In these trajectories, C–C dissociation of 1C occurred resulting in HCOH + HCO^-. The HCOH carbene, upon formation, immediately isomerized to HCHO or dissociated to H_2 + CO products. In the 9 and 13 eV simulations, 4 and 6 trajectories, respectively, resulted in HCHO + HCO^-, however, HCO^- further dissociated to H^- + CO products in some of these trajectories. Similarly, we did not observe the formation of CO + CH_3O^- (m/z = 31) products in these simulations. However, in the 13 eV simulation, 3 trajectories showed formation of CO + $^-CH_2OH$ (m/z = 31) products. The $^-CH_2OH$ is a higher energy isomer (by 36.7 kcal/mol) of CH_3O^- and resulted via C–C dissociation of 1C with concomitant hydrogen transfer. In a large fraction of trajectories in the low energy simulations, dissociation or isomerization of 1C was not observed. Snapshots of example trajectories showing these different reaction pathways are shown in Fig. 4. Numbers inside each frame is time in fs at which the snapshot was taken. Formation of H_2O + $HCCO^-$ products can be seen in 4(a) wherein C–O dissociation and hydrogen transfer can be observed in the 584 and 633 fs frames, respectively. 4(b) shows an example intramolecular hydrogen transfer trajectory wherein the hydrogen shifts can be seen in the 213 and 2460 fs frames.

3.4. Dynamics of 1O

Dissociation dynamics of the slightly higher energy 1O isomer was quite different from that of 1C discussed above. The *retro*-formose reaction, resulting in the HCO^- + HCHO products, was observed in these simulations in large fraction of trajectories. At E_{rel} = 2, 5, 9, and 13 eV, we observed 0, 53, 88, and 96 trajectories, respectively. This is a direct dissociation process with a reaction endoergicity of 52.2 kcal/mol (see Fig. 2) and the search for a dissociation transition state was unsuccessful. Visualization of the trajectories showed that the HCO^- + HCHO product formation from 1O occurs mainly via FFE or the shattering mechanism [38] i.e., C–C dissociation occurs within a very short time after the collision with the Ar atom. Non-shattering type 1O → HCO^- + HCHO reaction i.e., longer time gaps between collision and dissociation occurred only in a very small number of trajectories in the low energy simulations. Note that for the 1C isomer also, major reaction paths (H_2O elimination and the ketene channel) followed a shattering type mechanism. Subsequent dissociation of HCO^- + HCHO products was also observed in the high energy trajectories. Dissociation of HCO^- to CO + H^- occurred in 10 and 16 trajectories, at E_{rel} = 9 and 13 eV, respectively. Also, dissociation of HCHO to H_2 + CO occurred in a few trajectories in the high energy simulations (see Table 1). Snapshots of an example trajectory forming HCO^- + HCHO products are presented in Fig. 4(c). The C–C dissociation and the subsequent reaction of HCO^- forming H^- + CO can be observed in the 98 and 140 fs frames, respectively.

Experiments by Uggerud and co-workers [26] showed that a strong component at *m/z* = 31, corresponding to CH_3O^- product, was present in the CID spectra of deprotonated GA. In the present simulations, the reaction 1O → CO + CH_3O^- was observed in a small number of trajectories at E_{rel} = 5, 9, and 13 eV. Previous studies [26] and the present electronic structure theory

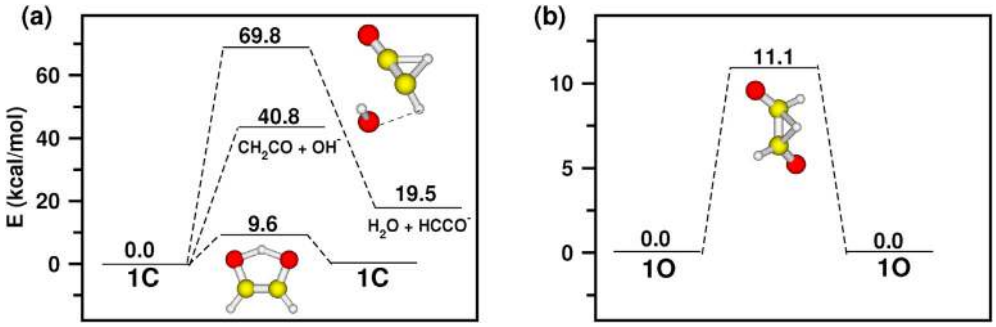

Fig. 3. Potential energy profiles for the reactions: (a) 1C → H_2O + $HCCO^-$, 1C → CH_2CO + OH^-, and intramolecular hydrogen transfer in 1C and (b) shows intramolecular hydrogen transfer profile for 1O.

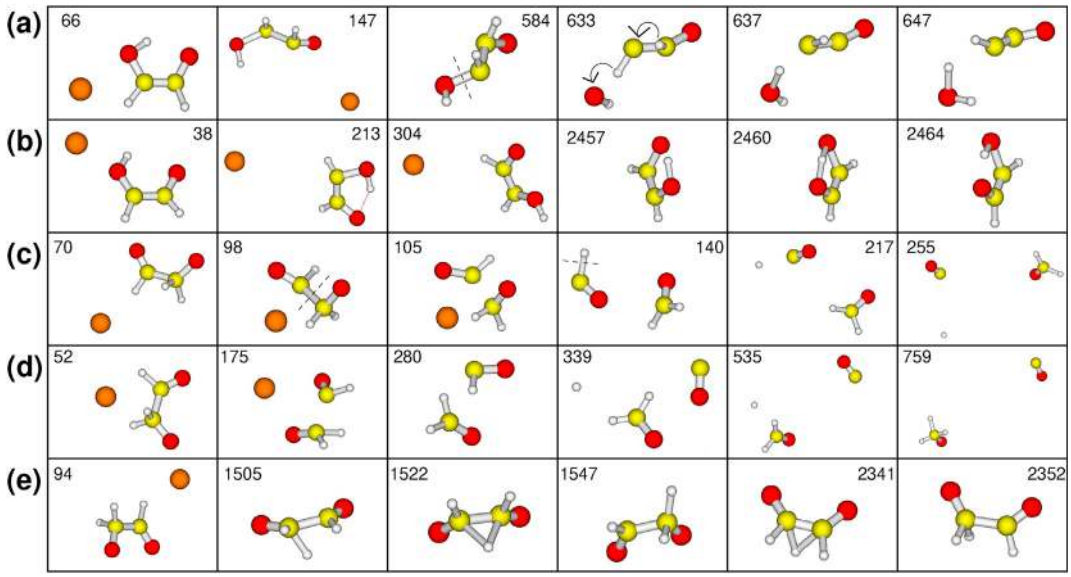

Fig. 4. : Snapshots of example trajectories showing the reaction (a) 1C → H_2O + $HCCO^-$, (b) 1C ↔ 1C, (c) 1O → HCO^- + HCHO → H^- + CO + HCHO, (d) 1O → HCO^- + HCHO → CO + CH_3O^-, and (e) 1O ↔ 1O. Numbers inside each frame is time in fs at which the snapshot was taken.

calculations (Fig. 2) show that the 1O → CO + CH_3O^- reaction occurs via a TS involving C—C bond dissociation with concomitant H atom transfer. This TS has a barrier of 32.1 kcal/mol relative to 1O. Interestingly, the trajectories that formed the CO + CH_3O^- products, though smaller in number, did not follow this pathway. They first underwent C—C dissociation resulting in HCHO + HCO^- products and after a small time period, H− transfer occurred from HCO^- to HCHO resulting in the final products. Snapshots of an example trajectory showing this pathway are given in Fig. 4(d). In this trajectory, HCO^- + HCHO formation occurs at 175 fs followed by HCO^- dissociation around 300 fs. The hydride ion moves around and attaches with HCHO forming CH_3O^-. Similar to 1C, intramolecular hydride transfer between the two C atoms of 1O was ubiquitous in the trajectories though the fractions were less in the latter in comparison to the former. Barrier for the hydrogen transfer is 11.1 kcal/mol relative to 1O computed using B3LYP/6-31+G* level of theory and the energy profile is shown in Fig. 3(b). Maximum number of trajectories showing this isomerization reaction was observed at $E_{rel} = 5$ eV. Snapshots of an example trajectory showing intramolecular hydrogen transfer is shown in Fig. 4(e). The hydrogen atom transfers can be observed in the 1522 and 2341 fs frames. The H_2O elimination channel and the ketene channel were observed in an appreciable fraction of trajectories in the dissociation of the 1C isomer however these channels were not important for 1O as there are no direct reaction pathways.

4. Discussion

CID experiments of deprotonated GA showed that the uncatalyzed, gas phase formose reaction HCO^- + HCHO → $HCOCH_2O^-$ is an unlikely event [26]. Electronic structure calculations show that the lowest energy isomer of deprotonated GA (1C) does not have a direct reaction pathway to form the *retro*-formose products. Consistently, direct dynamics simulations of 1C dissociation showed formation of HCO^- + HCHO only in a small number of trajectories. On the other hand, the slightly higher energy 1O isomer resulted in the desired reaction products in a large number of trajectories. The reaction involves direct C—C dissociation without a transition state and requires energy of 52.2 kcal/mol relative to 1O. In an infrared spectroscopic photolysis study, Niki et al. [13], found that OH radical primarily deprotonated GA from the carbonyl carbon and the other carbon atom to a yield of up to 80%. Deprotonation from the hydroxyl group of GA results in 1O from which the *retro*-formose products HCO^- + HCHO were mainly produced in the simulations. The 1O species formed only in least amounts in the experiments by Niki et al., and the branching ratios between these isomers were also confirmed in another study [44]. These observations indicate that the deprotonation of GA in the experiments by Uggerud and co-workers [26] may have primarily resulted in the 1C isomer and the formation of HCO^- + HCHO products required further isomerization from 1C → 1O and this reaction has a barrier of 46.2 kcal/mol. Lower 1O fractions observed in these experiments is probably why less *retro*-formose products were observed in the CID experiments by Uggerud and co-workers [26]. Another important observation in the present work is that the intramolecular hydrogen (hydride) transfer was ubiquitous in the simulations. Energy barriers were of the order of 10 kcal/mol and was observed in appreciable number of trajectories especially in the 5 eV simulations. Note that intramolecular hydride shift has been invoked in the proposed mechanism of formose reaction in a recent experimental study [4].

Table 2 shows a direct comparison of the product ions produced in the experiment and simulations. Clearly, there are differences between the simulation results and CID experiments [26]. In particular, experiments showed larger peak intensity for the $m/z = 31$ signal in comparison to $m/z = 29$ signal. In the simulations, $m/z = 31$ species (CH_3O^- or $^-CH_2OH$) resulted in a smaller number

Table 2
A Comparison of the Simulation and Experimental Results in Terms of the *m/z* Values of the Ions Observed.

m/z	simulation	experiment[a]
29	yes	yes
31	yes	yes
57	no	yes
41	yes	no
17	yes	no
59	yes	yes

[a] From reference 26.

of trajectories than m/z = 29 (HCO^-). This discrepancy may be rationalized as follows. Simulations showed that the CH_3O^- + CO products formed via HCO^- + HCHO products followed by intermolecular hydrogen transfer. In the simulations, a large fraction of trajectories resulted in HCO^- + HCHO products but they separated immediately upon formation. In the experiments, multiple collisions and the proximity of the products (HCO^- + HCHO) in the collision cell might have led to the larger CH_3O^- fractions. To a small extent, m/z = 57 ion (dehydrogenation product) was detected in the experiments but was not observed in the simulations. Differences [38] in the abundance of product ions between experiments and chemical dynamics simulations can occur because simulations were performed under single collision conditions but the experiments might involve multiple collisions. Furthermore, shattering is typically overestimated in simulations and there are timescale differences between simulations (in ps) and experiments (up to ms). It is also important to mention here that the impact parameter for the collisions were taken to be zero in the simulations. Hence, the simulations reported here may be viewed as describing fast fragmentation events occurring in the reaction in short time scales.

5. Summary

Classical chemical dynamics simulations modeling previously reported collision induced dissociation experimental study of deprotonated glycolaldehyde are reported. The experimental study was performed to understand the gas phase reaction between formyl anion and formaldehyde in the interstellar media to form carbohydrates. The study concluded [26] that the efficiency for this reaction is low and the results of the present simulations are in qualitative agreement with this work. Deprotonation of GA can occur at three different sites and the dynamics simulations were performed for the lowest energy 1C isomer and slightly higher energy 1O isomer. The *retro*-formose reaction GA → HCHO + HCO^-, occurred mainly from the slightly higher energy 1O isomer via a direct C–C dissociation. CID of the lowest energy 1C isomer resulted in the *retro*-formose products only in a very small number of trajectories. Analysis of the trajectories showed non-statistical nature of the dissociation dynamics of deprotonated glycolaldehyde.

Declaration of competing interest

The authors declare that they have no known competing financial interests or personal relationships that could have appeared to influence the work reported in this paper.

Acknowledgement

Funding from Department of Science and Technology, India, through grant number CRG/2019/000454 is acknowledged. The lead author of the paper expresses his sincere gratitude to Prof. William L. Hase for his guidance and support during the author's stay in Prof. Hase's research group and thereafter.

Appendix A. Supplementary data

Supplementary data to this article can be found online at https://doi.org/10.1016/j.ijms.2020.116468.

Conflicts of interest

The authors declare no conflicts of interest.

References

[1] A. Butlerow, Bildung einer zuckerartigen substanz durch synthese, Justus Liebigs Ann. Chem. 120 (1861) 295.
[2] R. Breslow, On the mechanism of the formose reaction, Tetrahedron Lett. 1 (1959) 22.
[3] A. Ricardo, F. Frye, M.A. Carrigan, J.D. Tipton, D.H. Powell, S.A. Benner, 2-Hydroxymethylboronate as a reagent to detect carbohydrates: application to the analysis of the formose reaction, J. Org. Chem. 71 (2006) 9503.
[4] C. Appayee, R. Breslow, Deuterium studies reveal a new mechanism for the formose reaction involving hydride shifts, J. Am. Chem. Soc. 136 (2014) 3720.
[5] A.F. Jalbout, L. Abrell, L. Adamowicz, R. Polt, A.J. Apponi, L.M. Ziurys, Sugar synthesis from a gas-phase formose reaction, Astrobiology 7 (2007) 433.
[6] T. Wang, J.H. Bowie, Radical routes to interstellar glycolaldehyde. The possibility of stereoselectivity in gas-phase polymerization reactions involving CH_2O and CH_2OH. Org. Biomol. Chem. 8 (2010) 4757.
[7] D.T. Halfen, A.J. Apponi, N. Woolf, R. Polt, L.M. Ziurys, A systematic study of glycolaldehyde in Sagaittarius B2(N) at 2 and 3 mm: criteria for detecting large interstellar molecules, Astrophys. J. 639 (2006) 237.
[8] P.M. Woods, G. Kelly, S. Viti, B. Slater, W.A. Brown, F. Puletti, D.J. Burke, Z. Raza, On the formation of glycolaldehyde in dense molecular cores, Astrophys. J. 750 (2012) 19.
[9] P.M. Woods, B. Slater, Z. Raza, S. Viti, W.A. Brown, D.J. Burke, Glycolaldehyde formation via the dimerization of the formyl radical, Astrophys. J. 777 (2013) 90.
[10] I. Magneron, R. Thevenet, A. Mellouki, G. Le Bras, G.K. Moortgat, K. Wirtz, A study of the photolysis and OH-initiated oxidation of acrolein and trans-crotonaldehyde, J. Phys. Chem. 106 (2002) 2526.
[11] X. Zhou, G. Huang, K. Civerolo, J. Schwab, Measurement of atmospheric hydroxyacetone, glycolaldehyde, and formaldehyde, Environ. Sci. Technol. 43 (2009) 2753.
[12] R.J. Yokelson, R. Susott, D.E. Ward, J. Reardon, D.W. Griffith, Emissions from smoldering combustion of biomass measured by open-path Fourier transform infrared spectroscopy, J. Geophys. Res. 102 (1997) 18865.
[13] H. Niki, P.D. Maker, C.M. Savage, M.D. Hurley, Fourier transform infrared study of the kinetics and mechanisms for the chlorine-atom-and hydroxyl-radical-initiated oxidation of glycolaldehyde, J. Phys. Chem. 91 (1987) 2174.
[14] C. Bacher, G.S. Tyndall, J.J. Orlando, The atmospheric chemistry of glycolaldehyde, J. Atmos. Chem. 39 (2001) 171.
[15] A. Beeby, D.B.H. Mohammed, J.R. Sodeau, Photochemistry and photophysics of glycolaldehyde in solution, J. Am. Chem. Soc. 109 (1987) 857.
[16] C. Zhu, L. Zhu, Photolysis of glycolaldehyde in the 280-340 nm region, J. Phys. Chem. 114 (2010) 8384.
[17] W. Chin, M. Chevalier, R. Thon, R. Pollet, J. Ceponkus, C. Crépin, Photochemistry of glycolaldehyde in cryogenic matrices, J. Chem. Phys. 140 (2014) 224319.
[18] J.P. Porterfield, J.H. Baraban, T.P. Troy, M. Ahmed, M.C. McCarthy, K.M. Morgan, J.W. Daily, T.L. Nguyen, J.F. Stanton, G.B. Ellison, Pyrolysis of the simplest carbohydrate, glycolaldehyde (CHO-CH_2OH), and glyoxal in a heated microreactor, J. Phys. Chem. 120 (2016) 2161.
[19] J.M. Hollis, F.J. Lovas, P.R. Jewell, Interstellar glycolaldehyde: the first sugar, Astrophys. J. 540 (2000) L107.
[20] J.M. Hollis, P.R. Jewell, F.J. Lovas, A. Remijan, Green bank telescope observations of interstellar glycolaldehyde: low-temperature sugar, Astrophys. J. 613 (2004) L45.
[21] M.T. Beltrán, C. Codella, S. Viti, R. Neri, R. Cesaroni, First detection of glycolaldehyde outside the galactic center, Astrophys. J. 690 (2009) L93.
[22] J. Li, Z. Shen, J. Wang, X. Chen, D. Li, Y. Wu, J. Dong, R. Zhao, W. Gou, J. Wang, S. Li, Widespread presence of glycolaldehyde and ethylene glycol around sagittarius B2, Astrophys. J. 849 (2017) 115.
[23] M. De Simone, C. Codella, L. Testi, A. Belloche, A.J. Maury, S. Anderl, P. André, S. Maret, L. Podio, Glycolaldehyde in Perseus young solar analogs, Astron. Astrophys. 599 (2017) A121.
[24] M.K. Sharma, A.K. Sharma, M. Sharma, S. Chandra, Anomalous absorption in glycolaldehyde in a cosmic object, N. Astron. 45 (2016) 45.
[25] S. Thripati, R.O. Ramabhadran, Metal-Ion-and Hydrogen-Bond-Mediated interstellar prebiotic chemistry: the first step in the formose reaction, J. Phys. Chem. 121 (2017) 8659.
[26] O. Sekiguchi, E. Uggerud, Fragmentation of deprotonated glycolaldehyde in the gas phase and relevance to the formose reaction, J. Phys. Chem. 117 (2013) 11293.
[27] I.A. Papayannopoulos, The interpretation of collision-induced dissociation tandem mass spectra of peptides, Mass Spectrom. Rev. 14 (1995) 49.
[28] L. Sun, W.L. Hase, Born-Oppenheimer direct dynamics classical trajectory simulations, Rev. Comput. Chem. 19 (2003) 79.
[29] M. Paranjothy, R. Sun, Y. Zhuang, W.L. Hase, Direct chemical dynamics simulations: coupling of classical and quasiclassical trajectories with electronic structure theory, WIREs Comput. Mol. Sci. 3 (2013) 296.
[30] M. Valiev, E.J. Bylaska, N. Govind, K. Kowalski, T.P. Straatsma, H.J.J. Van Dam, D. Wang, J. Nieplocha, E. Apra, T.L. Windus, et al., NWChem: a comprehensive and scalable open-source solution for large scale molecular simulations, Comput. Phys. Commun. 181 (2010) 1477.
[31] G.H. Peslherbe, H. Wang, W.L. Hase, Monte Carlo sampling for classical trajectory simulations, Adv. Chem. Phys. 105 (1999) 171.

[32] C. Schlier, A. Seiter, Symplectic integration of classical trajectories: a case study, J. Phys. Chem. 102 (1998) 9399.
[33] C. Schlier, A. Seiter, High-order symplectic integration: an assessment, Comput. Phys. Commun. 130 (2000) 176.
[34] W.L. Hase, R.J. Duchovic, X. Hu, A. Komornicki, K.F. Lim, D. -h. Lu, G.H. Peslherbe, K.N. Swamy, S.R. Vande Linde, A. Varandas, et al., VENUS. A general chemical dynamics computer program, Quant. Chem. Prog. Exch. Bull. 16 (1996) 671.
[35] X. Hu, W.L. Hase, T. Pirraglia, Vectorization of the general Monte Carlo classical trajectory program VENUS, J. Comput. Chem. 12 (1991) 1014.
[36] U. Lourderaj, R. Sun, S.C. Kohale, G.L. Barnes, W.A. De Jong, T.L. Windus, W.L. Hase, The VENUS/NWChem software package. Tight coupling between chemical dynamics simulations and electronic structure theory, Comput. Phys. Commun. 185 (2014) 1074.
[37] S.J. Klippenstein, A.L.L. East, W.D. Allen, A high level ab initio map and direct statistical treatment of singlet ketene, J. Chem. Phys. 105 (1996) 118.
[38] A. Martin Somer, V. Macaluso, G.L. Barnes, L. Yang, S. Pratihar, K. Song, W.L. Hase, R. Spezia, Role of chemical dynamics simulations in mass spectrometry studies of collision-induced dissociation and collisions of biological ions with organic surfaces, J. Am. Soc. Mass Spectrom. 31 (2020) 2.
[39] G.L. Barnes, A. Shlaferman, M. Strain, Fast fragmention during surface-induced dissociation; an examination of peptide size and structure, Chem. Phys. Lett. 754 (2020) 137716.
[40] E. Martínez-Núñez, A. Fernández-Ramos, S.A. Vázquez, J.M. Marques, M. Xue, W.L. Hase, Quasiclassical dynamics simulation of the collision-induced dissociation of $Cr(CO)_6^+$ with Xe, J. Chem. Phys. 123 (2005) 154311.
[41] E. Martínez-Núñez, S.A. Vázquez, J.M. Marques, Quasiclassical trajectory study of the collision-induced dissociation of CH_3SH^+ + Ar, J. Chem. Phys. 121 (2004) 2571.
[42] Y.J. Chen, P.T. Fenn, K.C. Lau, C.Y. Ng, C.K. Law, W.K. Li, Study of the dissociation of $CH_3SCH_3^+$ by collisional activation: evidence of nonstatistical behavior, J. Phys. Chem. 106 (2002) 9729.
[43] E. Martínez-Núñez, S.A. Vázquez, F.J. Aoiz, J.F. Castillo, Quasiclassical trajectory study of the collision-induced dissociation dynamics of Ar + CH_3SH^+ using an ab initio interpolated potential energy surface, J. Phys. Chem. 110 (2006) 1225.
[44] I. Magneron, A. Mellouki, G. Le Bras, G.K. Moortgat, A. Horowitz, K. Wirtz, Photolysis and OH-initiated oxidation of glycolaldehyde under atmospheric conditions, J. Phys. Chem. 109 (2005) 4552.